

GT2015-43322

COMPETING 3D MECHANISMS IN COMPRESSOR FLOWS

James V. Taylor and Robert J. Miller

Whittle Laboratory, University of Cambridge, United Kingdom

Email: jvt24@cam.ac.uk

ABSTRACT

Even though three-dimensional design is central to all modern compressor design systems, many of these methods still rely, at their core on a two-dimensional, sectional, view of blade aerodynamics. This paper argues that this view fundamentally limits design by not correctly considering the way in which pressure gradient transverse to the flow direction affects both separation and loss.

The first part of the paper details how 3D blade stacking and the transverse pressure gradient fundamentally alters the behaviour of the corner separations and trailing edge separations. By controlling this design parameter it is possible to switch between the two. The transverse pressure gradient is also shown to be responsible for a substantial increase in profile loss.

In the second part this understanding is used to explore the uncertainty of the design space by simultaneously varying pitch-chord ratio and 3D stacking. It is shown that the design space is split in half by two different levels of risk.

INTRODUCTION

Even though three-dimensional design is central to all modern compressor design systems, many of these methods still rely, at their core, on a two-dimensional, sectional, view of aerodynamics. This paper will argue that this view fundamentally limits design because it does not capture the true loss mechanisms and fluid phenomena which shape the real design space.

At the early stage of the design process two-dimensional compressor aerodynamics still plays a central role. Blade sections are often designed using quasi-3D methods such as MISES. These methods are typically used to both minimise profile loss and to inform pitch-chord ratio selection.

Later in the design process, during the 3D phase, designers are still encouraged to interpret the CFD in a 2D way. An example of this is the endwall diffusion parameter and corner stall metric proposed by Lei et al. in [1]. At its heart this metric is two-dimensional, comparing the performance of a 2D section close to the endwall to the midspan. Even during the final stages of the design process, when the 3D blade geometry is being developed, the designer is encouraged to

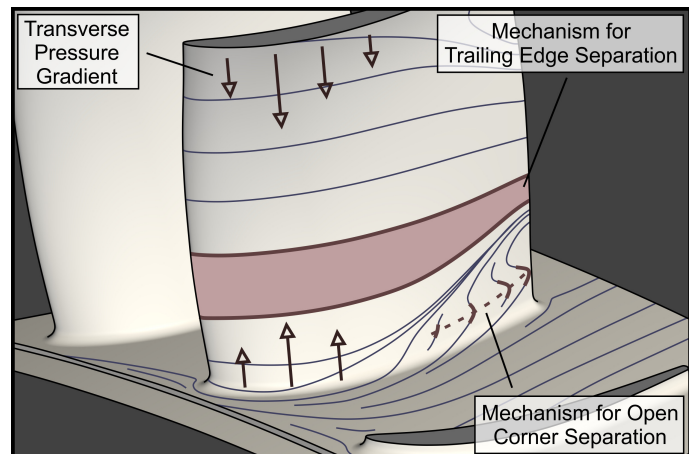


FIGURE 1. TRANSVERSE PRESSURE GRADIENT CONTROLS COMPETITION OF 3D FLOW MECHANISMS

interpret the CFD in a 2D way. An example is when compound lean is said to off-load the endwall sections relative to the midspan section.

The main property of a 3D flow is the capacity for its boundary layer to develop a transverse component, whereas in two-dimensions it is constrained to remain in plane. The existence of the third dimension offers the boundary layer the possibility of “escape” laterally when it is confronted with an adverse streamwise pressure gradient. This lateral “escape” means that the streamwise pressure gradient experienced by the boundary layer in a 3D flow is often lower than that experienced in a 2D flow. Considering aerodynamics in a 2D sectional way therefore misses the central behaviour that differentiates two-dimensional and three-dimensional flow.

The main outcome of 3D design should be to “manage” the transverse component of the boundary layer flow by controlling the transverse pressure gradients. Two-dimensional thinking completely ignores the central role of transverse pressure gradients in design.

In this paper it is shown that the two failure mechanisms, which limit the operating incidence range of an blade, are both 3D in nature, and that the onset of each mechanism can be controlled by manipulation of the surface transverse pressure gradient. The two mechanisms

are shown in Figure 1. The transverse pressure gradient created by the blade's 3D design is shown as a number of open arrows.

The first failure mechanism is an open corner separation. The region for the mechanism's onset is labelled in Figure 1. The limiting surface streamlines can be seen to reverse in direction in the closed corner separation. This will be shown later in the paper to directly result in the onset of an open corner separation. The transverse pressure gradient acts to control the reversal of the limiting streamlines.

The second failure mechanism is a 3D trailing edge separation. This mechanism is traditionally thought to be two-dimensional or quasi-three-dimensional. In this paper it will be shown to be caused by differential transverse migration of boundary layer fluid relative to the freestream. Once again the transverse pressure gradients are directly responsible for controlling the magnitude of this differential migration.

In this paper it is also shown that the loss mechanisms which control the design incidence performance of the blade are also 3D. This means that in the presence of the transverse pressure gradient the profile loss becomes 3D in its nature and cannot be predicted using 2D or quasi-3D methods.

This paper will argue compressor design should be undertaken by extracting these 3D mechanisms from the 3D CFD and balancing them to achieve an optimal design.

The one remaining problem with this novel approach to 3D design is uncertainty. The CFD may drive the designer to take out some compound lean or to remove blades in the search for improved performance. However, the designer is always uncertain of whether the numerically predicted benefits will be achieved in reality.

To answer this question, in the second part of the paper the design space, described by simultaneous variation of 3D stacking and of pitch-chord ratio, is experimentally explored. It is shown that the design space is split into two regions based on the underlying 3D failure mechanisms described in Figure 1. In the first region the uncertainty is high and the designer must seek extensive experimental validation of the design. In the second region the uncertainty is shown to be low and the designer should have more confidence in being guided by the predictions of the CFD.

1 METHOD

The datum stator geometry considered in this paper is taken from the low speed single stage Gibbons research compressor at the Whittle Laboratory. It is a low speed design of a rear stage from a high pressure compressor. Pitch-chord ratio and 3D stacking are varied simultaneously to give the 15 blades considered in this paper. 3 levels of pitch-chord ratio are selected; 100%, 108% and 116% of the datum value. The 3D stacking profiles are scaled linearly from the datum design in 5 levels; 30%, 70%, 100%, 130% and 170%. This scaling results in blades with true lean angles at the hub of 6°, 14°, 20°, 26° and 34°. True sweep angles at the hub are 1.2°, 2.8°, 4°, 5.2° and 6.8°. The stacking angles are those made by the intersection of the line of centroids of each section with the hub in the directions of true lean and sweep; normal and parallel to the chord as in [2]. The datum stator of the Gibbons compressor operates with an inlet midspan Mach number of 0.3 and Reynolds number of 350,000. The aspect ratio is 1.1 and hub to tip ratio is 0.85.

Numerical

The CFD results presented in this paper are all computed using TURBOSTREAM. It is a structured multi-block RANS solver based upon TBLOCK and implemented for parallel GPU operation. Further details and validation are given in [3]. Most results are from steady simulations of the rotor and stator rows coupled with a mixing plane, the results not of this configuration are detailed in the text. An experimental area traverse of the IGV exit is used at the rotor inlet. The turbulence model used was the Spallart-Allmaras method [4]. The meshing process is automated using AUTOGRID. The total cell count for the two rows is 3.1 million with 105 spanwise points and 19 in the rotor tip gap. y^+ is lower than 1 on all walls at all operating points. In the stator row a butterfly fillet topology was used at both hub and casing to ensure no discontinuity in angle and improve the accuracy of the flow in the endwall suction surface corner. Transition was not modelled and the code considers the flow fully turbulent on all surfaces.

Experimental

The Gibbons compressor is a vertical axis machine located at the Whittle Laboratory. A rapid testing facility has been developed that enables 3D printed cured resin stator cassettes to be replaced in sectors. The blade geometry and endwalls are printed together as the same part resulting in a shrouded configuration. The stator and rotor hub platforms are sealed to ensure that no leakage path exists between the rows. Experimental results given in this paper are based upon stator inlet and exit traverses undertaken with a five-hole pneumatic probe. The ratio of probe diameter to span is 1.8% and the stator exit traverse is taken 0.25 chords downstream of the trailing edge. Stator geometry is replaced in sectors of 1/5 of an annulus, equivalent to 15 blades, the central two are traversed. Static-static stator characteristics are measured using 36 pneumatically averaged casing tappings spaced over the central 3 pitches of the 1/5 annulus sector at both inlet and exit of the stator row.

2 3D BLADE DESIGN

The purpose of the 3D design method used in this study is to vary the transverse pressure gradient on the blade while maintaining the same spanwise distribution of loading for all designs.

The traditional view of 3D stacking is presented in the top panel of Figure 2. When compound lean is applied to a blade of constant section the isobars within the passage are said to remain radial. The cross passage pressure gradient is strongest nearest the suction surface. This means the effect of the lean reduces the loading at the endwalls while it increases at midspan. Comparing the two designs in the top panel it is clear to see that the low 3D design has an almost constant spanwise loading distribution while the high 3D design has a different number of isobars at midspan and endwalls. For a constant blade section this view of 3D design is correct. The problem with this method of 3D design is that the spanwise loading distribution and the transverse pressure gradients on the blade surface are coupled.

The aim of this study is to use 3D design to vary the transverse pressure gradients while holding the spanwise loading distribution constant. By redesign of the blade's camber it is possible to alter the loading and flow turning through another method. For all of the 3D stacking profiles used in this paper the blade's camber has been redesigned to maintain the same flow turning at all spanwise

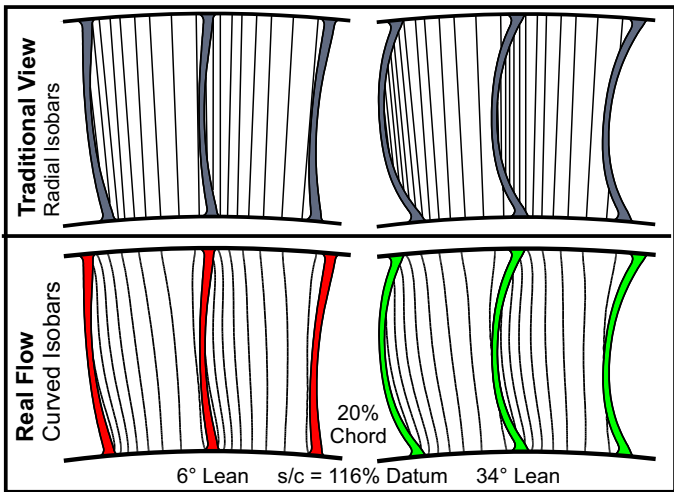


FIGURE 2. TRADITIONAL AND REAL VIEWS ON THE EFFECTS OF 3D STACKING DEMONSTRATED BY CONTOURS OF CONSTANT STATIC PRESSURE IN A MID CHORD CUT OF THE PASSAGE

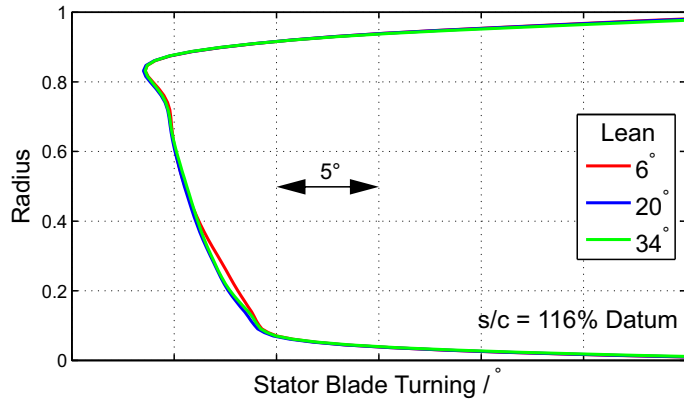


FIGURE 3. FLOW TURNING EQUAL TO THE INLET GAS WHIRL ANGLE MINUS THE EXIT

locations. Additionally the shape of the blade pressure distributions is held constant: the chordwise position of peak suction, the leading edge incidence and boundary layer shape factor distribution on the rear of the blade are maintained at all spanwise locations.

The effect of this design method on the mid passage isobars is shown in the lower panel of Figure 2. The first result to note is that the isobars are curved. The second is that in the comparison between the isobars of the 6° lean design on the left and the 34° lean case on the right it is seen that the number of isobars is the same for both at the hub, but also at midspan and the casing.

The ability to maintain the loading and lift distribution is further demonstrated by the flow turning distributions presented for three designs in Figure 3. It is possible to achieve any physical spanwise loading distribution with any 3D stacking profile using the above method.

The second aim of this design method used in this study is to design blades with varying pitch-chord ratios. In the design of a row of blades for different pitch-chord ratios it is impossible to maintain the magnitude of the loading; each blade must have a higher loading to achieve the desired flow turning. In this case it is again the shape of the pressure distribution and spanwise distribution of flow turning that is held constant.

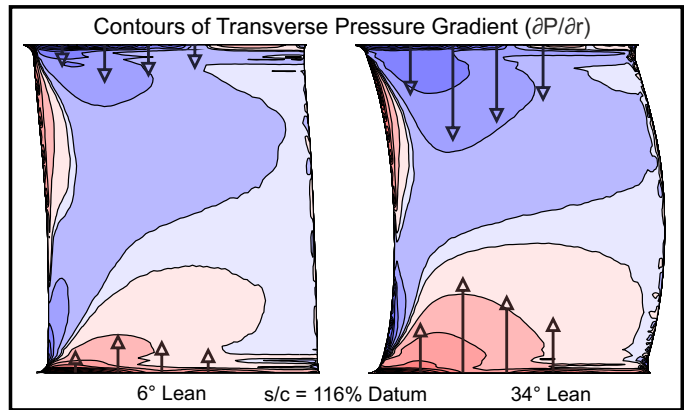


FIGURE 4. 3D STACKING INCREASES THE MAGNITUDE OF THE TRANSVERSE PRESSURE GRADIENT

The result is a design method which allows transverse pressure gradient on the blade surface to be varied independently of other design parameters. The only difference between any two given designs in this paper is the strength of this transverse pressure gradient. Figure 4 shows contours of the transverse pressure gradient, equal to the radial pressure gradient in this constant annulus case, for two different blades.

The transverse pressure gradient acts to force flow from both the hub and casing endwalls towards midspan, in the case of the 34° lean geometry the transverse pressure gradient is markedly stronger. The varying strength of pressure gradient with lean angle controls the transverse motion of flow on the suction surface and the topology of the closed corner separations. This is the mechanism by which all of the phenomena described below are controlled.

3 3D FLOW MECHANISMS

The aim of this section is to use 3D CFD calculations of a set of blade designs to describe the effects of the transverse pressure gradient on the 3D flow. In particular the nature of the 3D aerodynamic failure and loss generating mechanisms will be investigated.

The results of Figure 5 are used to introduce the specific problems which will be answered in this section. The results of this figure are cast in terms of 4 questions which will be answered in the 4 different subsections of this half of the paper:

1. In Figure 5 the blade with 34° lean fails at a lower incidence than the blade with 20° of lean. The failure mechanism of both of these blades is characterised by the progressive separation of the suction surface boundary layer at the trailing edge. The effect of this separation can be seen in the downstream loss contours plotted for 3 incidences in the upper panel of Figure 6. The question answered in the first section is: How does 3D stacking affect the transverse flow to cause early separation?

2. In Figure 5 the blade with 6° lean fails by the sudden opening of a corner separation at the critical incidence of 5.3°. The other more highly 3D blades do not. The flow structure before and after the critical incidence is shown in the lower panel of Figure 6. Two questions are answered in the second section: What causes the opening of the corner separation to occur for only low 3D designs and is it possible to quantify the stability of the corner separation?

3. In Figure 5 the blade with 34° lean has 2.2% higher loss than

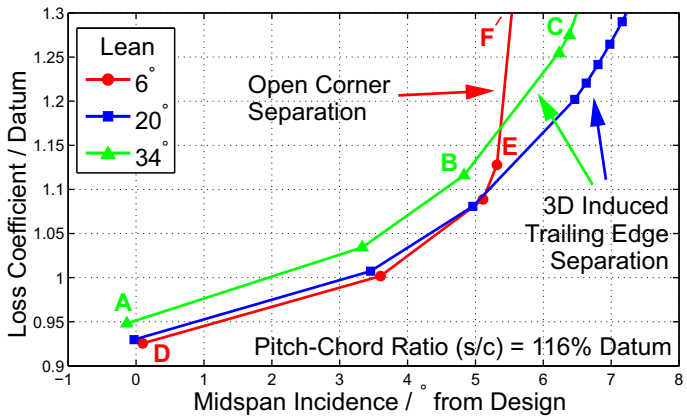


FIGURE 5. 3D TOTAL LOSS LOOPS SHOWING THE EFFECT OF 3D STACKING ON THE FLOW MECHANISMS

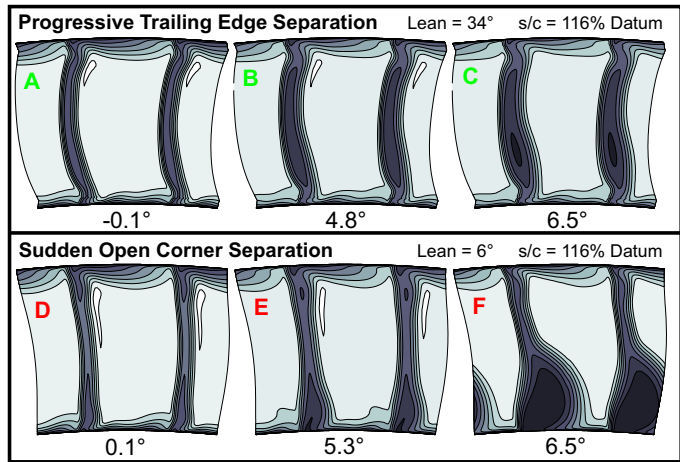


FIGURE 6. CONTOURS OF LOSS COEFFICIENT ILLUSTRATE 2 DIFFERENT FAILURE MECHANISMS

the blade with 6° lean. This is due to an increased profile loss as is evident in the wake depths in the two contour plots at the design incidence in Figure 6. How does the transverse flow on the suction surface cause the profile loss to become 3D in nature and rise in magnitude?

4. While the profile loss rises due to the transverse flow the loss generated in the corner separations can be seen to fall in Figure 6. In the final subsection one question is addressed: How do the different loss components add up to result in the case that low 2D blades have lower total loss generation than 3D blades?

3D Trailing Edge Separations

An example of an blade which exhibits a 3D trailing edge separation is shown in Figure 7. Historically these separations have been treated in a 2D way; the boundary layer and free stream are considered to be confined in the same plane. In the 3D flow this is not the case. At the design incidence the blade in the left panel of Figure 7 exhibits strong transverse flow towards midspan. This is caused by the transverse pressure gradients set up by the design's 34° of compound lean. As the incidence is raised, in the right panel, a combination of streamwise diffusion and differential transverse flow causes the trailing edge boundary layer to separate. In practice this often happens close to the closed corner separations and the blade "unzips" up the span.

The magnitude of the transverse pressure gradient in a design is

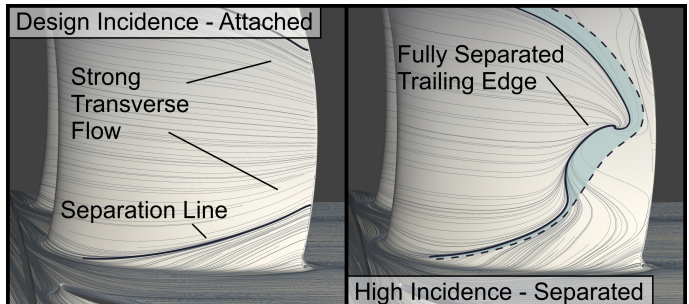


FIGURE 7. FLOW TOPOLOGY OF A TRAILING EDGE SEPARATION IN THE 34° LEAN, S/C = 116% OF DATUM

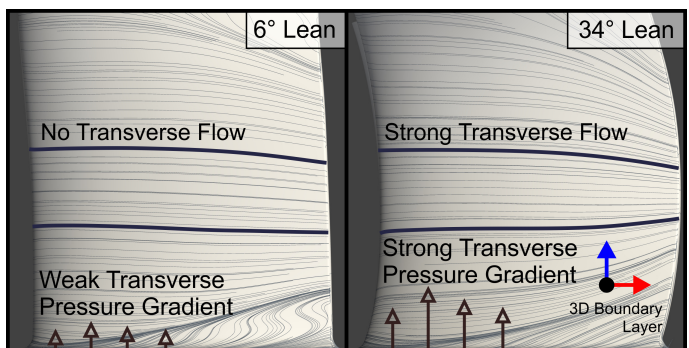


FIGURE 8. DIFFERENCE IN SPANWISE FLOW FOR TWO DIFFERENTLY STACKED DESIGNS AT S/C = 116% OF DATUM

determined by the level of 3D stacking. Figure 8 shows two blades; one with 6° lean and low transverse pressure gradient the other with 34° lean and a strong transverse pressure gradient. The blade with 34° lean is observed to separate at the trailing edge at a lower incidence than the design with 6° of lean. The suction surface limiting streamlines at 40% and 60% span are highlighted. For the blade with 6° lean the magnitude of the transverse velocity in the boundary layer is observed to be small, while for the design with 34° of lean the magnitude of the transverse velocity in the boundary layer is observed to be large.

The differential transverse migration between the boundary layer and freestream fluid can be seen in Figure 9. The figures show the streamwise and transverse components of velocity of the boundary layer at the point marked in black in Figure 8. The effect of transverse pressure gradients is to overturn the low streamwise momentum fluid. The fluid closest to the wall has the lowest streamwise momentum and can therefore be seen to incur the largest transverse velocity component.

The effect that the differential transverse flow of boundary layer fluid has on the shape factor of the boundary layer at the trailing edge is shown in Figure 10. The left panel of the figure shows the contraction ratio of the limiting surface streamlines. The surface contraction ratio is calculated between neighbouring surface streamlines from leading to trailing edge. The right panel shows the consequent effect on the boundary layer shape factor at the trailing edge. It is clear from the figure that as the 3D stacking is increased, the increase in transverse pressure gradient results in a more significant contraction of the limiting surface streamlines. The increased contraction rate indicates more low streamwise momentum fluid is fed transversely towards midspan. This acts to make the boundary layer more inflectional and closer to separation and corresponds to a rise in trailing edge shape

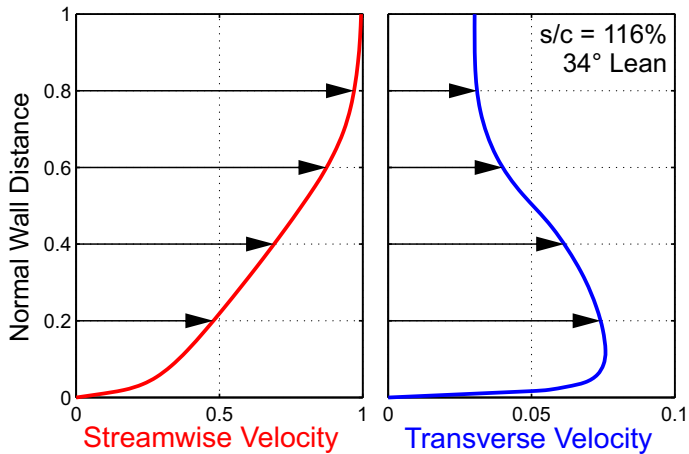


FIGURE 9. 2 COMPONENTS OF A 3D BOUNDARY LAYER ON A 3D BLADE

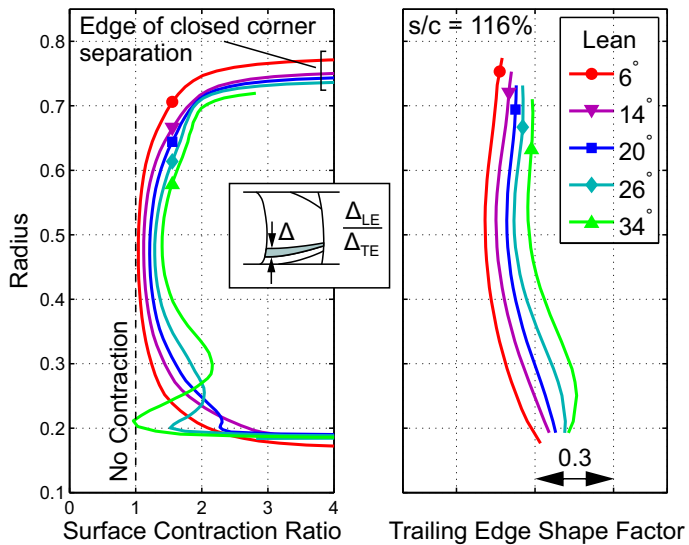


FIGURE 10. DETRIMENT TO BOUNDARY LAYER STABILITY IS QUANTIFIED IN 3D CFD

factor. The effect of changing lean from 6° to 34° was observed in this case to change the trailing edge boundary layer shape factor by 0.3.

On the separation line marking the edge of the closed corner separation (20% and 75% radius) the contraction rates become very high but no increase in boundary layer shape factor is observed. Along this line the endwall boundary layer and suction surface boundary layer meet and flow is pulled off of the surface. This acts to stabilise the boundary layers by removing the low streamwise momentum fluid into the freestream. The authors currently do not have a method of quantifying this effect.

The effect of the transverse pressure gradient in degrading the stability of the suction surface boundary layers is seen to be substantial, between the lean angles of 6° and 34° an increase in shape factor of 0.3 is recorded locally. Reliance on a 2D view which does not take this mechanism into account will result in a significant overprediction of the operating range of 3D stacked designs.

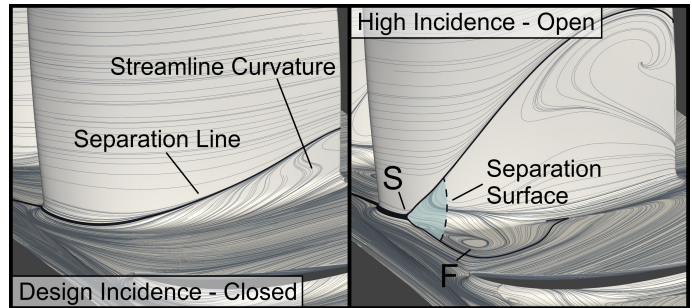


FIGURE 11. TOPOLOGY OF CLOSED AND OPEN CORNER SEPARATIONS

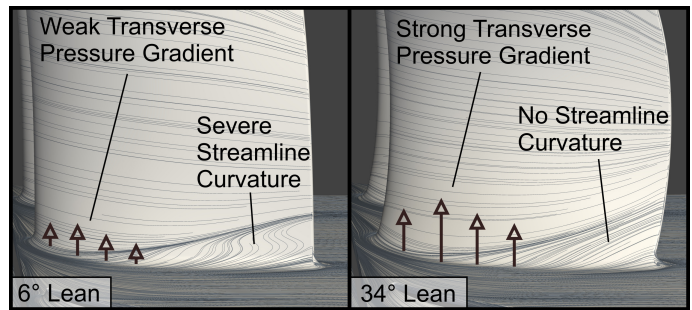


FIGURE 12. DIFFERENCE IN STREAMLINE CURVATURE FOR TWO DIFFERENTLY STACKED DESIGNS AT $S/C = 116\%$ OF DATUM

Open Corner Separations

An example of a blade which fails by an open corner separation is shown in Figure 11. At the design incidence in the left panel of Figure 11 the blade exhibits a closed endwall separation. Close to the hub trailing edge corner, on the suction surface is a region marked as high streamline curvature. This is a region of the boundary layer fluid which has been reversed by the streamwise pressure gradient. It will be shown that this is the region of the flow that the open corner separation originates from. At high incidence, in the right panel of Figure 11, the blade exhibits an open corner separation. The formation of this topology requires the opening of a "separation surface". Open corner separations occur only on blades with low levels of 3D stacking.

The presence of the separation surface is the single feature which distinguishes between a closed corner separation and the open type. The separation surface divides the flow in the passage as shown in the right panel of Figure 11. At the root of this surface on the blade itself is a saddle point marked as "S" and on the endwall a focus exists, marked "F". Closed corner separations are identified only by the presence of the "separation line", this can exist without any reversed flow. A complete definition of 3D separation lines and surfaces is given by Délery in [5]. For the flow topology to switch from a closed to an open separation requires the production of saddle point and focus pair.

The magnitude of the transverse pressure gradient on a blade surface is determined by the level of the blade's 3D stacking. Figure 12 shows two blades one with 6° of lean and the other with 34° of lean. The effect of adding lean increases the transverse pressure gradient and acts to remove the region of severe streamline curvature close to the suction surface hub corner. It achieves this by transporting the overturned low streamwise momentum fluid from the endwall boundary layer up the span and out of the corner. The region of high streamline curvature is where the open separation originates and

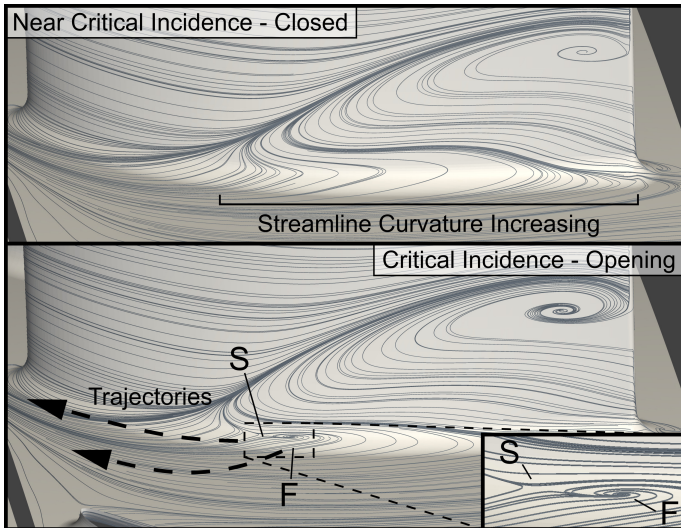


FIGURE 13. INSTANTANEOUS SNAPSHOTS OF THE LIMITING SURFACE STREAMLINES BELOW AND ABOVE THE CRITICAL INCIDENCE

therefore 3D stacking acts to deter the formation of open separations.

In order to investigate the significance of the severe streamline curvature as an origin for the transition of the corner separation from closed to open a URANS solution was used to model the flow as the incidence is increased through the critical value accurately. A multi-passage domain with 6 stators of the datum pitch-chord ratio and a lean of 6° was selected, the upstream IGV and rotor rows were also included with sliding planes. One stator in the 6 was modified to have 1% less lean than the others. This ensures that only one stator reaches its critical incidence first. This method is similar to that employed by Pullan et al in [6] in their treatment of spike-type compressor stall.

The incidence was raised to the critical value and the topology of the corner separation is presented before and after the saddle point and focus pair have formed in Figure 13. In the first panel it is noted that the curvature of the reversing streamlines has increased dramatically as the incidence is been raised from the design value. This is caused by the increase of both the streamwise adverse pressure gradient on the suction surface and the cross passage pressure gradient that drives the low momentum endwall boundary layer fluid across the passage. At the root of the corner separation, on the fillet, at approximately 40% chord, the curvature of the streamlines is most severe. When the incidence is raised fractionally above the critical value the curvature becomes infinitely sharp as the streamlines are reversed, this is the region in which the saddle point and focus pair are able to form.

In order to interpret the significance of this region of the flow in forming the open corner separation from the closed type it is necessary to refer to the theory of critical points first published by Poincaré in [7] and recently applied to corner separations in compressor blades by Gbadebo et al in [8]. Two parts of this theory are significant to explain the phenomena: Firstly, critical points, such as foci, saddles and nodes, can only form from other regions of singular shear stress. Secondly, the number of critical points in the flow field must obey Equation 1 at all instants in time. The symmetry of this equation results in the production of the saddle point and focus pair together.

$$\sum(Foci+Nodes) - \sum Saddles = 0 \quad (1)$$

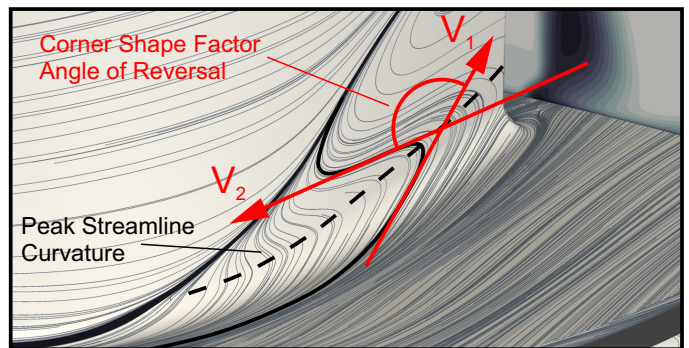


FIGURE 14. DEFINITION OF THE CORNER SHAPE FACTOR

The saddle point and focus pair originate from the region of infinitely sharp streamline curvature located on the fillet. The production of the two critical points is shown clearly in the lower panel of Figure 13, an instantaneous snapshot of the limiting surface streamlines. This pair of points has a separation line running between them. A separation surface now exists stretched between the existing and the new separation lines. Through this mechanism the separation surface is able to form from the centre of the blade suction surface. This ensures that the failure mode occurs suddenly without warning.

Once the two critical points have formed, the flow becomes unstable and unsteady and moves swiftly to achieve a new stable operating point. Ultimately the saddle point moves forward toward the leading edge while the focus separates from it to sit on the hub endwall, the separation surface stretches between them as in Figure 11 and blocks most of the passage. This results in the loading of the blade collapsing.

The CFD solution has 6 passages and at this time-step only one passage, with 1% less lean, has an open separation. The blockage in this passage acts to load up the neighbouring passage on the suction side. This causes this the neighbouring passage to exceed its critical incidence and the closed corner separation starts to open. This occurs until all of the passages have failed. The behaviour is identical to that used to describe the progression of stall cells described by Stenning in [9]. However, no stable rotating cells of open corner separations are found to occur in this domain of only 6 stator blades.

Now we have an understanding that the opening of the corner separation originates from a region of infinitely sharp streamline curvature it is possible to define a metric which measures the magnitude of this curvature. This metric is to called the “corner shape factor” as it’s concept is analogous to a 2D boundary layer shape factor in that is purely defined by the flow shape. It is a measure of how close a closed corner separation is to forming the separation surface

Local streamline curvature is difficult to measure robustly so the corner shape factor has been defined as the angle between the forwards facing flow vector (V_1) and the reversed flow vector (V_2), shown in Figure 14. The corner shape factor varies between 0 and π . Once the angle reaches π the local curvature of the streamlines reach has become infinitely sharp and the saddle and focus points form the separation surface.

To check the validity of this new metric the Figure 15 shows the new metric plotted against endwall loss for all 15 geometries considered in this paper at all incidences run. The endwall loss is defined as the loss in the 20% mass flow nearest the hub wall. A clear correlation can be seen between the shape factor and the

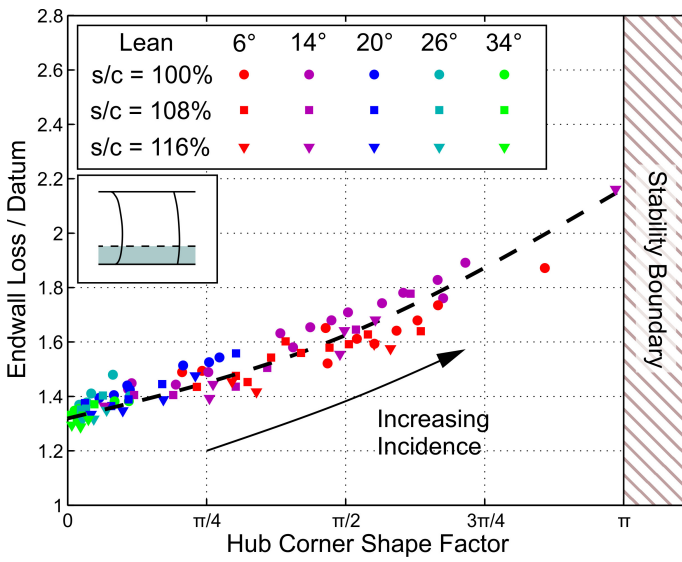


FIGURE 15. STABILITY AS DETERMINED BY CORNER SHAPE FACTOR FOR ALL GEOMETRIES AT ALL OPERATING POINTS

endwall loss. The corner shape factor ceases to have meaning once the separation has triggered to the open type and these results are not plotted. It should be noted that once the open separation formed the endwall loss exceeds that of the datum by 3 times.

Figure 15 also shows the effect of the transverse pressure gradient. At 34° of lean all the blades at all incidences have a hub corner shape factor of less than $\pi/8$. While at the designs at 20° of lean have a hub corner separation of only less than $3\pi/8$ at all incidences. The power of the corner shape factor is determining the proximity to the formation of the separation surface and therefore the stability of a closed corner separation on any blade is evident. The authors intend for this parameter to be used in design for this purpose, much the same way as a boundary layer shape factor is used in section design to determine its proximity to separation.

3D Profile Loss

The effect of 3D stacking on design incidence loss is observed in Figure 5. All of the blades considered have an identical loading distribution and therefore the extra loss at high levels of 3D must result from the transverse pressure gradient. To understand the cause of this change in loss the axial distribution of mass averaged stagnation pressure loss through vane was calculated and is shown in Figure 16. In order to investigate the change in profile loss only the calculation was performed for the central 20% mass flow. The loss at the trailing edge of the three blades rows can be seen to be very similar in magnitude. The mixing loss downstream of the blades can be seen to differ significantly.

To determine the overall loss a circumferential mixing calculation was undertaken at blade trailing edge. The values of the mixed out loss are shown as three dashed lines. It can be seen that a change in blade lean from 6° to 34° causes a rise in profile loss of 20%.

Figure 17 shows the streamwise vorticity downstream of the stators with 6° and 34° lean. As the lean of the blade is increased the transverse velocity component in the suction surface boundary layer goes up. This can be seen to raise the vorticity in the trailing edge wake. The secondary component of kinetic energy flux in the wake

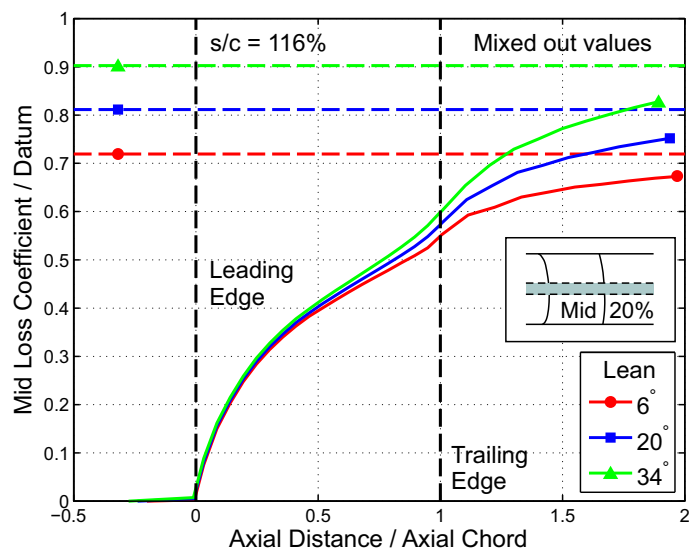


FIGURE 16. A DESCRIPTION OF PROFILE LOSS THROUGH THE STATOR ROW AND DOWNSTREAM

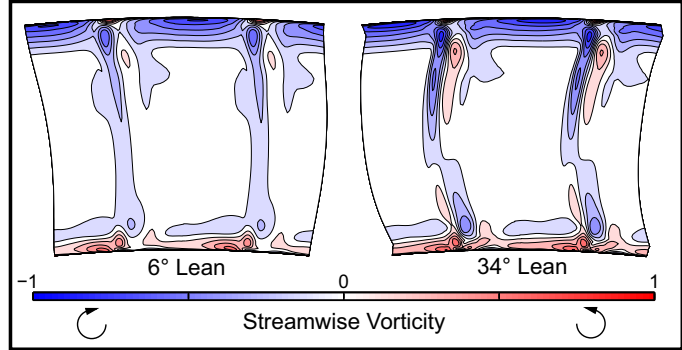


FIGURE 17. STREAMWISE VORTICITY GENERATED BY EXCESSIVE TRANSVERSE PRESSURE GRADIENT

was investigated to determine whether it could be responsible for part of the increase in downstream mixing loss. The total secondary kinetic energy doubles between the case of 6° lean and 34° lean. However, the absolute magnitude of the kinetic energy was found to be small compared to the mixing loss observed in Figure 16.

The other possible cause of increased mixing loss is an increase in the trailing edge H_{23} , the shape factor relating the momentum thickness and the energy thickness. The value of H_{23} therefore sets the downstream future mixing loss. Schlichting in [10] shows that for a turbulent boundary layer described by a power law there is a unique relationship between H_{23} and H_{12} (the ratio of displacement thickness to momentum thickness as shown in Figure 10). This relationship was found to only account for 30% of the difference observed in the CFD.

Total Loss

The change in total blade loss with the level of 3D stack is shown in Figure 18. The loss is split into “corner and endwall loss” defined as the 20% mass flow closest to each wall. The other 60% of mass flow is defined as “3D profile loss”. Between a lean of 6° and 34° the total loss was found to increase by just 2.2%. This contrasts to a large rise in 3D profile loss of 19% and large drop in endwall and corner loss of 9.6%. The relatively modest change in total loss with lean thus seems

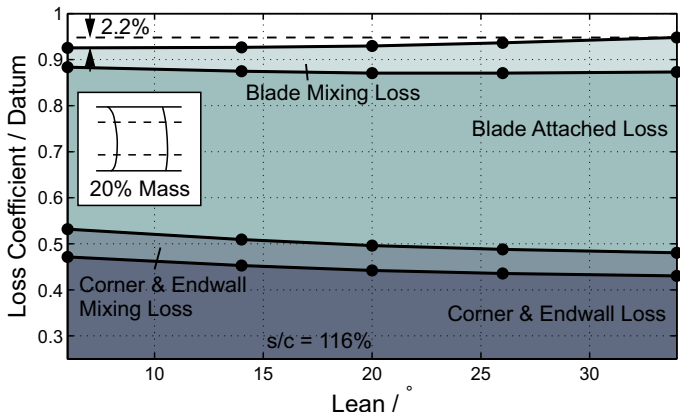


FIGURE 18. LOSS BREAKDOWN AS A FUNCTION OF 3D STACKING

to mask a significant rebalance of the loss distribution in the blade row.

If the mixing component of the 3D profile loss described in the above section were not taken into account then the total loss becomes an even weaker function of 3D stacking. If any optimisation were undertaken to determine an stacking profile to minimise the loss coefficient the design is likely to be non-optimal. It is the recommendation of this paper to optimise 3D stacking to give a transverse pressure gradient that balances the two failure mechanisms described above. In this case it is the operating incidence range that is maximised.

4 UNCERTAINTY IN REAL DESIGN

A compressor designer traditionally has one aerodynamic aim - To maximise design performance while maintaining the required operating incidence range. In reality there is a second and more important behaviour driving design, "risk". A designer may wish to increase pitch-chord ratio or reduce the amount of compound lean, in the search for design performance. However, such a choice risks catastrophic aerodynamic failure. In practice the designer is likely to react to this risk by "playing safe". In other words in practice a fear of "risk", a lack of understanding of uncertainty, is what inhibits innovative designs.

In this section the compressor design space is studied using both experiment and computation to investigate the level of uncertainty. The two design parameters varied are the pitch-chord ratio and the 3D stacking profile. The design space is interpreted using the mechanisms governing the aerodynamic 3D failure modes and loss generation described earlier in the paper.

The Design Space

The effect of varying pitch-chord ratio on design performance and incidence range will be introduced first. Figure 19 shows 3D CFD predictions of the loss loops of 3 pitch-chord ratio designs with 20° lean. The effect of raising pitch to chord ratio can be seen to reduce design loss while also causing the incidence range to narrow.

The whole design space, predicted by CFD, is shown in Figure 20. Two clear trends can be observed: First, at a fixed pitch to chord ratio there is a clear optimal level of lean which achieved the maximum operating range. Second, at a fixed lean increasing the pitch to chord always reduced the operating range. The designs of maximal operating range balance the two failure mechanisms, 3D

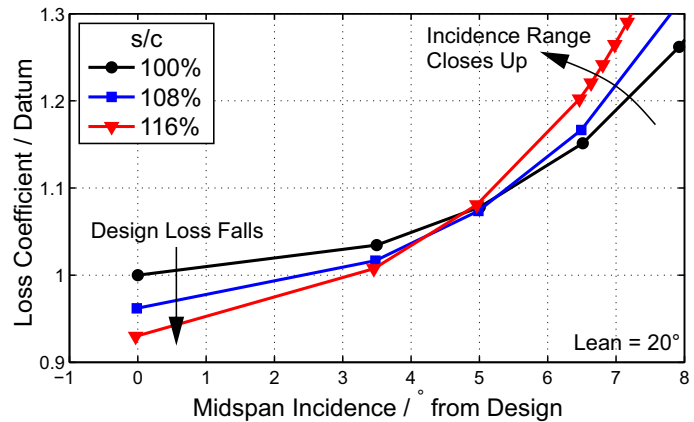


FIGURE 19. 3D TOTAL LOSS LOOPS SHOWING THE EFFECT OF PITCH-CHORD RATIO VARIATION

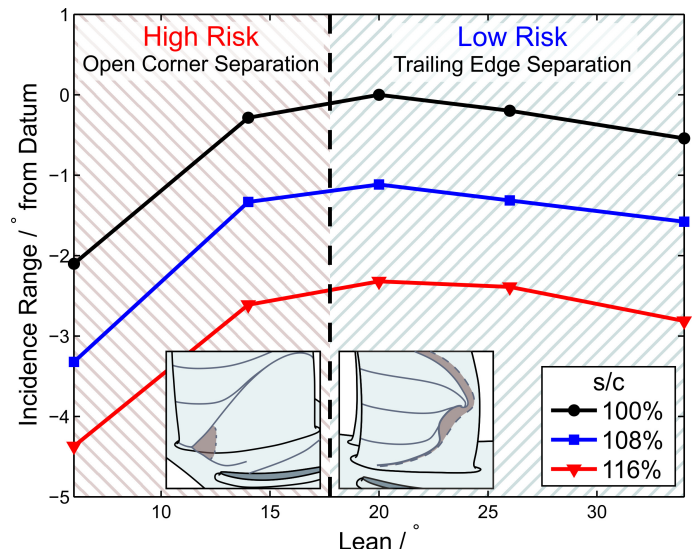


FIGURE 20. INCIDENCE RANGE FOR ALL 3D STACKINGS AND PITCH-CHORD RATIOS TESTED

trailing edge separation and open corner separation, through correct selection of the strength of the transverse pressure gradient.

Uncertainty in the ability of the CFD to predict the outcome of the experimental tests was found to vary across the design space; two levels exist and correlate with the type of failure mechanism. In the first region, where open corner separations control the incidence range, the uncertainty was found to be high with even small changes in inlet condition significantly changing the flow structure in the experimental test. In the second region, where 3D trailing edge separations control the incidence range, the uncertainty was found to be low with the trends in the CFD and experiment agreeing closely.

HIGH RISK - 2D DESIGN REGION

Over the entire "high risk" region the CFD and experiments were found to show significant discrepancy. In terms of the failure mechanism discussed earlier in the paper the biggest discrepancy was found to be the wall on which the open corner separation occurred.

To demonstrate this effect a single case will be presented. This case is characteristic of a designer attempting to maintain adequate range while reduce design incidence loss. In such a case the CFD

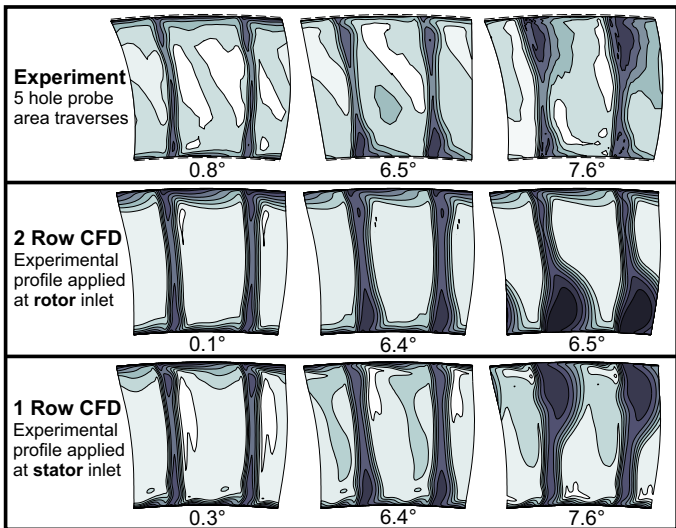


FIGURE 21. COMPARISON OF THE FLOW STRUCTURE FROM CFD AND EXPERIMENT FOR THE 6° LEAN, S/C = 108% DESIGN

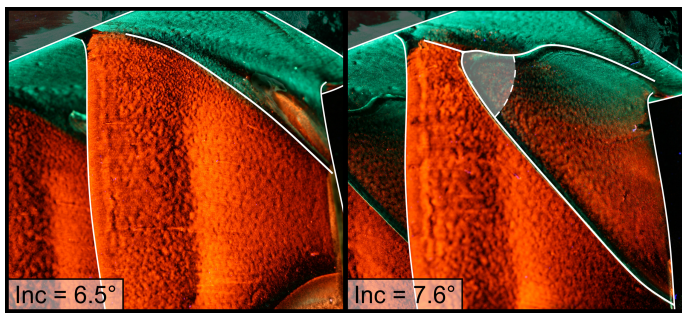


FIGURE 22. SURFACE FLOW VISUALISATION SHOWS THE TRANSITION OF A CLOSED CORNER SEPARATION TO THE OPEN TYPE FOR THE S/C = 108%, LEAN = 6° BLADE

shows that the designer would be sensible to reduce lean to 6° and increase pitch-chord ratio to 108% of the datum. The CFD predicts that these two choices combined reduces the total loss coefficient by 4.3% of the datum.

The experiment and CFD for the 6° lean, 108% pitch-chord ratio case is shown in Figure 21. The stator exit traverse at three incidences is shown in the first two rows of the figure. The first two incidences were selected to be the same for both CFD and experiment. The third was selected to be above the critical incidence, where the corner separation had just opened. The CFD is observed to accurately predict the experiment at the lower two incidences. However, at high incidences the CFD predicts the open corner separation occurring on the hub wall, instead of the casing, and at the wrong incidence by 1.1°.

The mechanism by which the corner separation opens on the casing wall is identical to that on the hub wall described by the CFD in the section above. Aside from the symmetry of the structure of the loss traverses in Figure 21 this result was confirmed by surface flow visualisation below and above the critical incidence. The predicted increased streamline curvature below the critical incidence and the separation surface of the open corner separation is illustrated in Figure 22.

The cause of this discrepancy between the location of the predicted open corner separation and the experiment was found to be a 3° error in the predicted stator inlet incidence between 80 and 90%

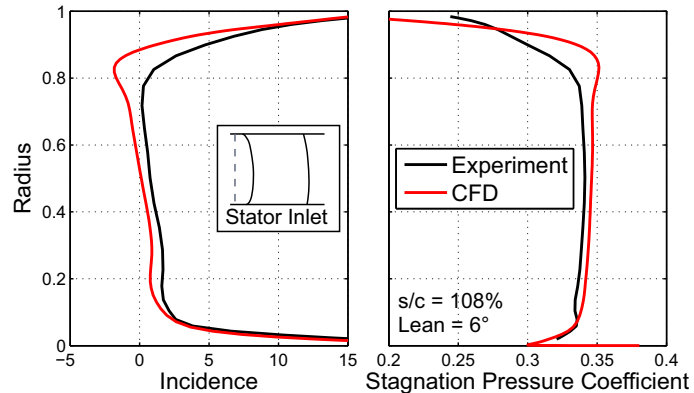


FIGURE 23. STATOR INLET PROFILE COMPARISON BETWEEN EXPERIMENT AND THAT PREDICTED BY CFD

span, this is shown in Figure 23. Inaccuracies in the CFD prediction of the upstream rotor in the region of the tip leakage flow have led to this difference in incidence and a corresponding error in the total pressure profile. It should be noted that a profile calculated from an experimental traverse was used to set the inlet conditions to the numerical simulation of the rotor.

To confirm the theory that the 3° error in stator incidence close to the casing was the cause of CFD inaccuracy in the stator row a single row CFD solution was run of a the stator alone. The stator inlet condition at each incidence was set using the experimental rotor exit traverses. The solution is plotted as the third row in Figure 21. It can be seen that the CFD and experiment now agree extremely well. The open corner separation occurs on the casing wall and the incidence at which the closed corner separation opens is accurately predicted.

The conclusion from these results is clear. In the “high risk” region, where failure is due to opening of a corner separation, the behaviour of the flow in a given row exhibits extreme sensitivity to the stator inlet conditions. In the case of a real multi-stage machine a greater uncertainty in the inlet profiles exists than that presented here. This increased uncertainty is due to the increased difficulty in measuring the profiles in a high speed machine, imperfect knowledge of the geometry and the cumulative errors that are built up in a multi-stage CFD calculation used for design.

LOW RISK - 3D DESIGN REGION

Over the entire “low risk” region the CFD and experiments were found to exhibit the same trends. Both the experiment and CFD was found to fail by a progressive trailing edge separation

To demonstrate this effect a single case will be presented. This case is characteristic of a designer attempting to maintain adequate range while reduce design incidence loss, but this time with the knowledge that they should keep out of the high risk region. The designer selects 20° of lean, enough to keep out of the high risk region. The designer then increases the pitch-chord ratio to 108% of the datum in an attempt to reduce design loss. The reason for not selecting 116% will become apparent later in the section.

The experiment and CFD for the 20° lean, 108% pitch-chord ratio design is shown in Figure 24. The loss coefficients from stator traverses are shown at exit for three incidences. The accuracy of the CFD is relatively good with the correct balance of trailing edge separation across the span captured.

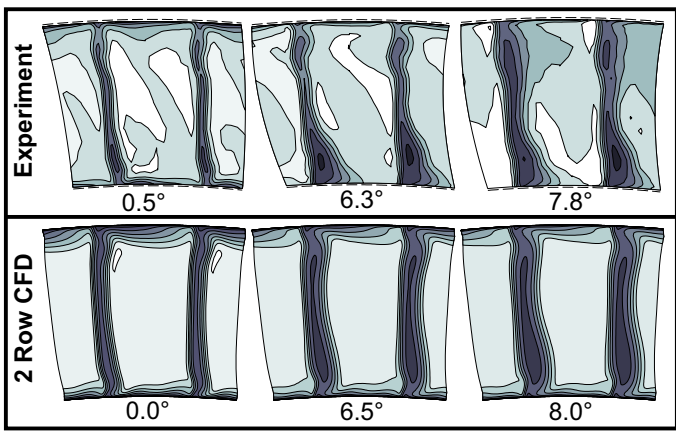


FIGURE 24. COMPARISON OF THE FLOW STRUCTURE FROM CFD AND EXPERIMENT FOR THE 20° LEAN, S/C = 108% DESIGN

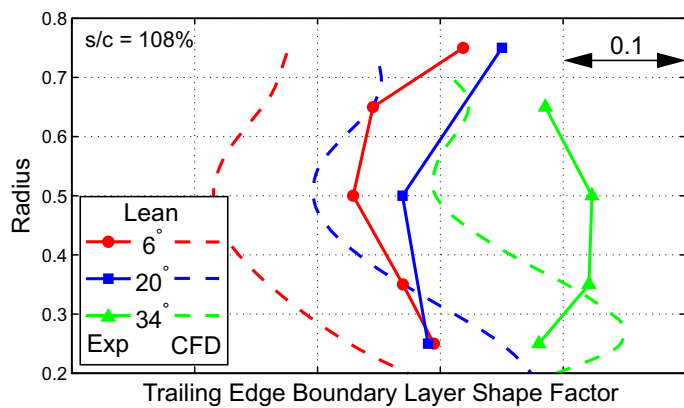


FIGURE 25. SPANWISE DISTRIBUTION OF TRAILING EDGE BOUNDARY LAYER SHAPE FACTOR FOR A RANGE OF DESIGNS

The question now turns to how well the CFD predicts the effects of transverse pressure gradient on the trailing edge shape factor of the boundary layer. To investigate this a flattened Pitot probe was used to measure 30 points across the boundary layer profile at the trailing edge. A comparison of the numerically predicted and experimental measured shape factors are shown in Figure 25.

The magnitude of the effect of transverse pressure gradient on trailing edge shape factor can be seen to be accurately predicted. A 0.15 rise in shape factor as lean is changed from 6° to 34° is recorded. The trend in the radial distribution of shape factor is also well predicted with a peak in shape factor occurring in the bottom 50% of span as the lean is raised to 34°. It should be noted that the absolute level of shape factor predicted by the CFD is low by 0.15. This indicates that reliance on CFD may lead a designer to raise the pitch-chord ratio too high.

Finally our attention turns to the selection of pitch-chord ratio. This is a difficult decision for a designer and needs to be made with full knowledge of available CFD and experiment. The prediction in loss coefficient at the design incidence is in error by no more than 1.5% of the datum value for all geometries. However, the discrepancy between the predicted operating range and experiment was found to rise steadily with increasing pitch-chord ratio.

The static pressure rise coefficient plotted against stator inlet incidence, for the 20° lean case, at three different pitch-chord ratios

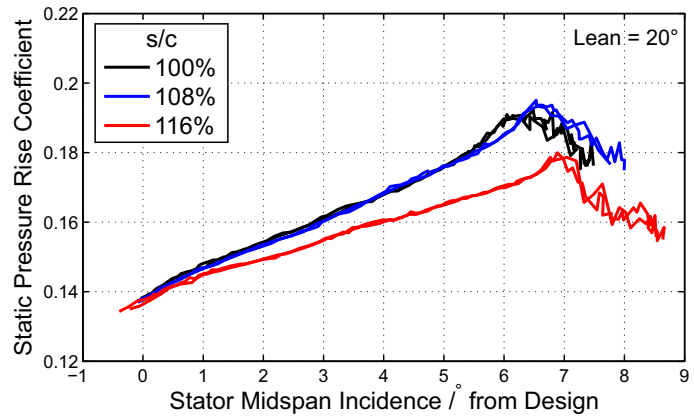


FIGURE 26. STATIC-STATIC STATOR CHARACTERISTICS SHOWING EXPERIMENTAL INCIDENCE RANGE VARIATION WITH PITCH-CHORD RATIO

is shown in Figure 26. All three geometries were designed in CFD to have identical static pressure rise coefficients at low and high incidence. The experimental results show all three designs made their design intent pressure rise but that the 116% pitch-chord ratio case significantly underperformed at more than 1° of positive incidence. If this highest pitch-chord ratio design were included in a multi-stage machine it would have a negative impact on the spool stability. For this reason the case considered earlier in the section was the 108% pitch-chord ratio.

The central message is therefore that in the “low risk” region greater trust can be put in the CFD to predict the correct trend in the underlying three-dimensional mechanisms. However, as pitch-chord ratio is reduced the discrepancy between CFD and experimental results grows in terms of trailing edge boundary layer shape factor and deviation. This indicates that if truly optimal designs are to be achieved the experimental validation is still required.

CONCLUSIONS

Two different 3D failure mechanisms have been shown to exist in axial compressor stators. Which one causes ultimate aerodynamic failure of the blade depends upon the strength of the transverse pressure gradient and therefore the 3D stacking profile:

1. A progressive trailing edge separation is common to blades with mid to high 3D stacking. The transverse pressure gradient causes an increased transverse movement of low streamwise momentum fluid towards the midspan. The suction surface boundary layer profile becomes more inflectional and separation occurs at a lower incidence. The effect was quantified through the use of the boundary layer shape factor calculated directly from the 3D CFD.
2. The sudden transition of a closed corner separation to an open type is common to blades with no or low 3D stacking. The lack of transverse pressure gradient increases the curvature of the limiting surface streamlines and a separation surface forms. The stability of a closed corner separation can now be quantified through the use of a new parameter - the corner shape factor.

The design space mapped out by variation in pitch-chord ratio and 3D stacking was found to be split in half by the tolerance of different designs to uncertainty. The two regions of the design space, a high and a low risk region, mapped to the two types of failure

mechanisms described above:

1. In the “high risk” region, where failures are due to open corner separations the flow on these blades exhibit extreme sensitivity to the stator inlet conditions. It should be noted that this is the region in which Goodhand and Miller in [11] found a significant sensitivity to roughness and leading edge geometry due to its effect on transition. It is clear that this is an area of the design space in which a designer has to be very brave, and well informed, to venture.
2. In the “low risk” region, where failures are due to trailing edge separations the flow on these blades is more robust to variation in inlet conditions. This region offers a safer mode of operation for designers to choose, however, this is at the expense of increased design loss.

The new way of viewing 3D design as a method to de-risk a compressor design project is an important finding of this work. However, at higher pitch-chord ratios, even in the “low risk” region the predictions of the CFD were found to diverge considerably from the results of the experiment.

In order to improve the management of uncertainty through the design process the experimental facilities should be moved closer to the designers and the rate of test increased. With modern 3D manufacture it is possible to test a new design in a matter of 1-2 days. This recommendation is in direct opposition to the current trend of moving facilities away from designers.

ACKNOWLEDGMENT

The authors would like to thank Rolls-Royce plc for their contributions and permission to publish this work, Chris Hall and Ian Bousfield for their invaluable advice, the EPSRC for their support, TURBOSTREAM for the use of their solver and Graham Pullan for his comments on 3D thinking.

REFERENCES

- [1] Lei, V.-M., Spakovszky, Z. S., and Greitzer, E. M., 2008. “A criterion for axial compressor hub-corner stall”. *Journal of Turbomachinery*, **130**(3), May, pp. 031006–031006.
- [2] Gallimore, S. J., Bolger, J. J., Cumpsty, N. A., Taylor, M. J., Wright, P. I., and Place, J. M. M., 2002. “The use of sweep and dihedral in multistage axial flow compressor blading part 1: University research and methods development”. *Journal of Turbomachinery*, **124**(4), Nov., pp. 521–532.
- [3] Brandvik, T., and Pullan, G., 2010. “An accelerated 3d navier stokes solver for flows in turbomachines”. *Journal of Turbomachinery*, **133**(2), Oct., pp. 021025–021025.
- [4] Spalart, P., and Allmaras, S., 1992. “A one equation turbulence model for aerodynamic flows.”. *AIAA Journal*, **94-439**, pp. –.
- [5] Délery, J., 2013. *Three-dimensional Separated Flow Topology*. ISTE Ltd and John Wiley & Sons Inc.
- [6] Pullan, G., Young, A. M., Day, I., Greitzer, E., and Spakovszky, Z., 2014. “Origins and structure of spike-type rotating stall”. *Journal of Turbomachinery*.
- [7] Poincaré, H., 1891. “Les points singuliers des équations différentielles”. *Comptes-Rendus de l'Académie des Science*.
- [8] Gbadebo, S. A., Cumpsty, N. A., and Hynes, T. P., 2005. “Three-dimensional separations in axial compressors”. *Journal of Turbomachinery*, **127**(2), May, pp. 331–339.
- [9] Stenning, A. H., 1980. “Rotating stall and surge”. *Journal of Fluids Engineering*, **102**(1), Mar., pp. 14–20.
- [10] Schlichting, H., and Gersten, K., 1999. *Boundary Layer Theory*. Springer.
- [11] Goodhand, M. N., and Miller, R. J., 2011. “The impact of real geometries on three-dimensional separations in compressors”. *Journal of Turbomachinery*, **134**(2), June, pp. 021007–021007.